-Title Page -

Slab buckling as a driver for rapid oscillations in plate motion and subduction rate

Erik van der Wiel[1*†], Jakub Pokorný [2*†], Hana Čížková [2], Wim Spakman[1], Arie P. van den Berg[1], Douwe J.J. van Hinsbergen[1]

1. Utrecht University
2. Charles University Prague

*Corresponding authors: Erik van der Wiel (e.vanderwiel@uu.nl) and Jakub Pokorny (jaakubpokorny@gmail.com)

† These authors contributed equally to this work

Abstract

Plate tectonics is primarily driven by the constant gravitational pull of slabs where dense oceanic lithosphere sinks into the mantle at subduction zones. Under stable plate boundary configurations, changes in plate motion are then thought to occur gradually. Surprisingly, recent high-resolution Indian plate reconstructions revealed rapid (2-3 Ma) plate velocity oscillations of ±50 %. Here we show, through numerical experiments, that the buckling of slabs in the mantle transition zone causes such oscillations. This buckling results from the deceleration of slabs as they sink into the lower mantle. The amplitude and period of buckling-associated oscillations depend on average subduction velocity and transition zone accommodation space. The oscillations also affect the upper plate which may explain enigmatic observations of episodic deformation and fluid flow in subduction-related orogens. We infer that the slab pull that drives plate tectonics is generated in just the top few hundred kilometers of the mantle.

Introduction

Plate kinematic reconstructions provide the quantitative constraints that underpin our understanding of the driving and resisting forces of plate tectonics: primarily slab pull and to a lesser extent ridge push as driving forces [1,2], and mantle drag as either driving or resisting plate motion (particularly by continental keels or slabs), and the resistance on subduction interfaces, as main additional forces [3-5]. An important constraint on plate reconstruction and relative plate motions since the Mesozoic is provided by marine magnetic anomalies that reveal plate motion change on various temporal scales. Reconstructions of major ocean basins usually provide one average Euler pole (plate motion data point) for stages of 3-10 Ma (e.g. [6], even though often more magnetic anomalies can be present in such stages. Such reconstructions reveal gradually changing plate motions on tens of millions of year time scales with occasional sudden cusps in plate motion between stages [7-9]. Gradual plate motion changes can be explained by changes in slab pull for example due to slow age variation of subducting lithosphere [10,11], or in the lubrication of plate contacts [3]. Cusps may correspond to changes in contributing forces through e.g., changes in slab pull due to subduction initiation or arrest [12,13], by slab detachment [14] or resistance to subduction of large oceanic plateaus [15], the arrival of a mantle plume-head that may lubricate or push plates [16,17], or to the decrease of a plate area through breakup (e.g.,[18]. Only recently, high-resolution (~0.5-1 Ma)

plate kinematic reconstructions of India-Africa spreading during the Eocene [19] revealed surprisingly variable ocean spreading kinematics.

It has long been known that the spreading rate between India and Africa, and the convergence rate between India and Asia, between ~65 and ~50 Ma, was very high, close to 20 cm/a [17,20]. Those estimates were based on about one Euler pole every ~5 Ma. White & Lister [21] suspected that shorter-wavelength plate velocity oscillations may have occurred although being smoothed out in existing global plate tectonic reconstructions. Their suspicion was recently corroborated by the high-resolution magnetic anomaly study of [19], which revealed that the period of high India-Asia convergence rate contained rapid oscillations with an amplitude 10 cm/a or more at a period of 6-8 Ma (Figure 1). Such plate motion variations suggest that a hitherto unrecognized process plays a role that causes oscillating changes in either slab pull, or friction, or both that perhaps becomes more pronounced with higher rates of subducting plate motion.

Subducting plate motions and changes therein must be accommodated in the underlying mantle. Correlations between imaged mantle structure and the global geological record of subduction show that the remnants of detached slabs in the lower mantle sink with rates of ~1-1.5 cm/a, almost regardless of the rate at which they subducted at a trench [22-24]. Therefore, subducting slabs eventually decelerate from plate tectonic rates (up to 20-25 cm/a [13,25] to average lower mantle sinking rates of <1.5 cm/a. To accommodate this requires some form of slab shortening or thickening. Subduction modelling revealed that this deceleration naturally leads to slab thickening, which could occur in the mantle transition zone through slab buckling [26-28]. Later, detailed tomographic analyses of slabs in the mantle transition zone and in the top of the lower mantle confirmed that they are systematically buckled [29,30]. Tomography of the lower mantle below India has revealed a major slab that is widely interpreted to represent the subducted Neotethys ocean, and that also contains the lithosphere that subducted between 65 and 50 Ma [31-34]. The enormous volume of this slab requires that it was drastically thickened, and while tomographic detail so far has not been able to resolve internal structure, the documentation that slabs buckle during thickening elsewhere [29,30] makes it feasible that this process also played a role here. Such buckling, which potentially may become more pronounced with faster subduction, makes slabs fold backward and forward, creating an oscillating slab dip and slab motion [35-41]. Here, we hypothesize that pronounced slab buckling causes the rapid, large-amplitude Eocene plate motion fluctuations of India.

To test this hypothesis, we conduct numerical experiments with decoupled, freely subducting plates that buckle in the mantle transition zone, creating periodically changing plate motions [42]. We evaluate under which conditions fluctuations such as those reported for the India plate may occur. We will discuss our results in terms of the implications for our understanding of the

driving forces of plate tectonics, and how obtaining detailed marine magnetic anomaly records may aid improving the predictive power of plate tectonic reconstructions for applications to plate boundary deformation and magmatic or mineralization processes.

Results

We conducted experiments in a 2D numerical model of subduction (Figure 2). The rheology of the upper and lower mantle [36,43,44] was chosen to accommodate typical subduction velocities [25] that in the upper mantle exceed the inferred lower mantle average slab sinking rates [23]. This mantle rheology leads to slab shortening and buckling in the upper-to-lower mantle transition zone (MTZ). We experimented with varying lithospheric ages to assess the effect of varying oceanic lithosphere thickness, and with varying crustal viscosities to assess the effect of average plate motion on the amplitude and period of the plate motion. We conducted one group of experiments, with a free overriding plate which leads to slab rollback and results in low angle buckling with multiple buckles (partly) present in above the 660 km discontinuity, and lower net lower mantle slab sinking rates (Figure 3a-g). Another group of experiments implements a fixed overriding plate that suppresses the development of rollback, such that subduction occurs at a mantle-stationary trench (Figure 3h-n). This generates buckling into a near-vertical slab-pile [45] that slowly sinks into the lower mantle leaving at any time only one buckle present above the 660 km discontinuity.

Slab shortening occurs through the combined resistance of the more viscous lower mantle and the endothermic phase change at the 660 km boundary, while the shallower part of the slab is continuously pulled by the exothermic phase change at 410 km (see methods). Buckling of the shortening slab is influenced by the non-linear rheology of the slab that results from the presence of a crust and lithospheric mantle layer [42]. We assess the horizontal velocity of the subducting plate V_{SP} and upper plate V_{UP} as an effect of lithospheric thickness (corresponding to the age of lithosphere at the trench) or through weakening subduction interfaces (crustal viscosity) to evaluate causal relationships between subduction dynamics and oscillating plate motions.

Slab buckling in the reference models

Figure 3 shows two reference experiments for the model setups with and without roll-back. These have a crustal viscosity of $10^{20}\ Pa \cdot s$ and overriding and subducting plate ages at the trench of 100 Ma. In the model with a mobile overriding plate (Figure 3 a-g), the slab undergoes a rapid, vertical descent through the upper mantle and the tip reaches the 660 km discontinuity after approximately 5 Ma model time (Supplementary Movie – panel A). The slab in the transition zone experiences down-dip compression which leads to (nonlinear) rheological weakening, causing the

slab to buckle forwards (Figure 4a) (i.e., towards the overriding plate) over the trapped tip that started to penetrate the 660 km discontinuity. Next, the slab buckles backward (i.e. towards the downgoing plate). This leads to an episode of roll-back and short-lived V_{SP} increase until the slab is almost vertically orientated at t = 11 Ma (Figure 4b). This is followed by the initiation of a second forward buckle, folding the slab over its deeper part in the MTZ, between t = 11 Ma and 18 Ma (Supplementary movie – panel A), associated with rollback and a decrease of V_{SP} and increase of V_{UP} (Figure 4b & 5a). This forward buckle starts tightening at t= 18 Ma, inducing the next backward buckle which is followed by a rapid increase of V_{SP} up to 12 cm/a, accompanied by a decrease of V_{UP} to almost 0 cm/a (Figure 5a). At t=20 Ma the next forward buckle initiated (Figure 3c), resulting again in an episode of rollback with decreasing V_{SP} and increasing V_{UP} (Figure 4a & 5a).

From here on, this process repeats itself quasi-periodically with new buckles forming approximately every 10 Ma (Figure 3c-f). This continuous subduction and rollback creates a buckled and thickened slab which slowly enters the lower mantle at an overall low-angle orientation (Figure 3d-g). After 70 Ma and 5000 km of subduction, the weak crust that facilitates the modelled subduction (see methods) is entirely consumed, the subducting plate is locked to the overriding plate and subduction stops. The modelled slab detaches and sinks into the lower mantle at a rate of ~1 cm/a, on par with inferred and modelled lower mantle slab sinking rates [23,43]. Throughout the experiment, and after 70 Ma of modelled convergence, the overriding plate and trench moved ~1000 km in absolute motion, i.e., relative to the mantle, towards the subducting plate.

The model with a fixed overriding plate, which suppresses rollback (Figure 3 H-N), shows similar characteristics. The slab is compressed down-dip and rheologically weakened in the transition zone, also resulting in the formation of a second buckle at around t=10 Ma (Figure 3i and Supplementary Movie – Panel B). The tightening of the buckle at the base of the upper mantle coincides with an increase in plate velocity around t=15Ma (Figure 5b). Due to the absence of rollback, the buckled slab is oriented vertically, like previously conceptualised ‘slab walls’ [27]. The oscillations in V_{SP} are of lower amplitude, on the order of 2 cm/a, recurring in a ~12 Ma period (Figure 5b). Absolute motion rates and oscillations therein of the subducting plate are similar to the scenario with roll-back but because the upper plate is fixed and roll-back does not add to the net convergence rate, subduction continued for ~90 Ma in model time, after which, the modelled slab detached and descended through the lower mantle with similar rate as in the reference model with rollback.

Plate motion oscillations caused by buckling

The quasiperiodic buckling of the subducting plate in the MTZ causes oscillations in the subduction velocity for both types of models (Figure 5) and in the motion of the overriding plate in the models that allow for roll-back (Figure 5a). Periods of fast V_{SP} coincide with tightening of a buckle and steepening of the slab and correspond with minima in the V_{UP} (Figure 5). We represent the periodicity of these plate motions with an amplitude and period, which we calculate in a 40 Ma time-interval of steady-state oscillations after subduction initiation and initial descend of the slab to the mantle transition zone, and before the end of the experiment (Figure 5). In the reference model with rollback, the subducting plate moved between 20 and 60 Ma with an average V_{SP} of 5.1 cm/a while oscillating between ~2 and 10 cm/a (Figure 5a). The average amplitude and period of the V_{SP} oscillations are 6.8 cm/a and 9.8 Ma (Figure 5a). Motion of the rigid, undeformable overriding plate, follows the oscillatory motion of the retreating trench. In the 20-60 Ma interval the overriding plate has an average V_{UP} of 1.8 cm/a towards the subducting plate, with oscillations between ~0 and 3 cm/a (Figure 5a). Maxima in trench motion and V_{UP} coincide with minima in V_{SP}, both occurring during formation of a new forward buckle and the associated shallowing of slab dip. During tightening of the buckle, the slab rolls back from inclined to vertical, associated with a sharp rise in V_{SP}, this change in angle is associated with a temporally near-stationary trench, and a resulting decrease in V_{UP} towards 0. The total convergence rate (V_C) then also oscillates (Figure 6a), with an amplitude of 6 cm/a, about 1 cm/a smaller than the amplitude of V_{SP}. The motion of the subducting plate accounts for 50-100% of the total convergence, while the overriding plate is only responsible for 50-0% (Figure 6b). The highest contribution of trench motion to the convergence occurs during periods of minimal V_{SP}.

The reference model with a fixed overriding plate (Figure 3h-n), so with a mantle-stationary trench, also shows oscillations in V_{SP} (Figure 5b) caused by the buckling of the overall vertical slab in the MTZ. In the 40 Ma long time-interval (here, between 30-70 Ma) quasiperiodic buckling occurs with an average V_{SP} of 5.7 cm/a (Figure 5b), faster than the model with rollback. The oscillations in V_{SP} occur with a period of 12.7 Ma and an amplitude of 1.6 cm/a. This amplitude is more than 4 times lower than the amplitude of oscillations in the model with rollback. The freedom to roll back allows for much larger variation in slab dips, and results in higher amplitudes of plate motion oscillations, as well as a higher net convergence rate.

How subduction velocity controls plate motion oscillations

When lithosphere subducts at a rate of 5-6 cm/a as in our reference models, it can reach the 660-discontinuity 13-11 Ma after passing the trench. Higher subduction rates decrease that time

interval and increase the amount of subducted slab in the MTZ, creating an accommodation space problem. We performed numerical experiments to evaluate the effect of subduction speed on the formation of buckles and on oscillations in V_{SP}. We modified the subduction rate in our experiments in two ways. On the one hand, we performed experiments with constant crustal viscosity while varying the age of the overriding and subducting plates. Overriding plate age determines the length of the subduction interface, with larger interfaces giving more resistance against subduction, decreasing subduction velocity. Subducting plate age determines the negative buoyancy, with higher subduction velocities for older plates [46]. On the other hand, we performed experiments with constant lithosphere ages (100 Ma) while adopting a constant or a power-law crustal viscosity, with lower viscosity yielding higher V_{SP} (e.g., [47]; see methods).

In our numerical experiments with varying plate age, the amplitude and period of the oscillations in plate velocity depend on the average subduction velocity (Figure 7, 8a-f). Models with a younger overriding plate and therefore a shorter subduction interface, have higher average subduction velocities within the 40 Ma long time-period with steady-state, quasi-periodic buckling (Figure 8 a,b). These velocities correlate directly to larger amplitudes (2-9 cm/a) in oscillations in the cases with rollback (Figure 8e). The cases with a stationary trench show that the amplitude of V_{SP} oscillations is predominantly determined by subducting plate age while the effect of the overriding plate age is limited. V_{SP} amplitudes vary between 1-3 cm/a (Figure 8f). Hence, faster-subducting plates have higher velocity amplitudes and lower periods of oscillation, and analogous to our reference models, this trend is most profound in models that allow rollback, in which the amplitudes are 2-3 times larger than in models with a mantle-stationary trench (Figure 7).

The models with a varying constant crustal viscosity show the same trend: higher average V_{SP}'s leads to larger velocity oscillation amplitudes (Figure 8 c,d) and smaller periods (Figure 8 g,h). Models with a power law crustal viscosity have smaller variations in average V_{SP} between them than those with a constant viscosity and consequently also smaller variations in oscillation amplitudes, albeit with higher absolute amplitudes (Figure 8 c,d). This is the result of feedback mechanisms between subducting plate velocity and the power law crustal viscosity [42], which also keeps the period of V_{SP} oscillations constant (Figure 8 g,h).

Discussion

Slabs that subduct with plate motions exceeding the average lower mantle sinking rate of 1-1.5 cm/a [23] inevitably require that slabs shorten and thicken. Interpretations of geophysical observations and subduction models (cited above), including our own, show that this occurs through

buckling of the slab in the MTZ (Figure 3). During slab buckling, the slab dip in the top ~300 km alternates between steep (vertical or overturned) and inclined, and our results illustrate that this induces alternating phases of slab rollback and stagnation (or advance), as well as motion of the trench and upper plate (Figure 5a). Our results reveal that these alternating phases of forward and backward buckling induce variations in subduction rate and subducting plate motion.

High subduction rates occur in our experiments when the slab buckles backward, towards the downgoing plate and adjacent to a previous slab fold. For backward buckling, the accommodation space in the MTZ in which the buckling slab can sink is available as opposed to forward buckling, in which case the lower part of the MTZ is still occupied by previously buckled slab (Figure 4a). As the 410 km phase transition enhances the negative buoyancy of slabs and thus enhances slab pull [36] the accommodation in the MTZ for backward buckling allows the slab to force a short (in our reference model < 3 Ma) pulse of high V_{SP}, and roll-back. During roll-back, the slab steepens to a vertical orientation accompanied by limited motion of the trench (Figure 4b), or even trench advance if the upper plate rheology would allow it. Once the slab overturns the next forward buckle initiates, during which time MTZ accommodation space decreases. A forward buckle is associated with trench retreat and slab advance in the MTZ, seemingly rotating over a pivot point in the upper mantle (Figure 4a). As a result, V_{SP} decreases during a forward buckling slab while V_{UP} increases. As the slab flattens during this forward buckle it creates accommodation space for the next backward buckle and associated acceleration (Figure 4b).

V_{SP} variations in models with a forced stationary trench are smaller because the slab has less variation in the amount of accommodation space in the MTZ. Trench-stationary subduction causes the slab buckling in a vertical column (Figure 3i-n). Basically, the rate and amplitude of plate motion oscillation primarily depends on the average V_{SP}: the higher, the bigger the space accommodation problem for slab folds in the MTZ. Our experiments with a moving trench and an average V_{SP} of 6 cm/a, i.e., the global average plate velocity [48], reveal rapid oscillations (< 10 Ma periods) with large V_{SP} fluctuations (3 to 13 cm/a) (Figure 6).

The rapid subducting plate motion oscillations that we find in our experiments have similar periods to those recently observed in the high-resolution (0.5-1 Ma) reconstruction of marine magnetic anomalies of the Indian Ocean [19]. Previous plate reconstructions using stage rotations based on larger stage intervals of 5-10 Ma (Figure 2) [6,17] smoothed out such rapid plate motion changes [21,49]. We illustrate this by sampling V_{SP} in our reference experiment with a mobile upper plate: when we sample on a 1-2 Ma resolution, similar to [19]) we resolve rapid (< 5 Ma) oscillations in plate motion caused by slab buckling (Figure 9a). However, sampling our V_{SP} curves at larger,

typically used intervals of 5 or 10 Ma generates the smooth plate motion history that is widely inferred from plate reconstructions (Figure 9 b,c).

The average V_{SP} as well as the amplitudes of the plate motion oscillations for the case of India are higher than in our experiments. These differences are likely at least in part explained by the simplicity of our model: the absolute plate motion rate of India may have been much higher than we obtained in our experiments because the Indian plate may have been lubricated at the base by a mantle plume [17,50], or the subduction interface may have been heavily lubricated by sediments [3]. The buckling behaviour may have differed because Indian subduction rates were not uniform along-strike, but increased eastward [17] and the lithosphere in the MTZ during the 55-50 Ma ago interval during which the oscillations were reconstructed may have been of continental origin [51]. This could have influenced the effects of the MTZ on slab pull, the rate of slab transfer into the lower mantle, and the amount of accommodation space in the MTZ, which would all influence the oscillation V_{SP} amplitude and period in our experiments.

An additional difference with our simple experiments is that subduction of the Indian plate occurred at a trench that was not retreating, as in our experiments, but instead slowly moving northwards, i.e. advancing [51]. In our experiments, subduction at a mantle-stationary trench occurs with lower amplitude oscillations than those reconstructed by [19]. However, the Indian slab may have advanced below the upper plate and retreated without significantly affecting trench motion as in our experiments. Slab buckling combined with trench advance could create an opposite regime as in our experiments, with acceleration during forward buckles and vice versa. Trench motion can even alternate between retreat and advance [52]. This could explain the ~1000 km wide north to south tomographic anomaly widely interpreted as the Indian slab [34]. We foresee that these processes may produce variations in MTZ accommodation space even when the trench is nearly stationary. Modelling such additional complexities is beyond the scope of our investigation: with the even higher subduction rates for India than we reproduced in our experiments, the space problem in the MTZ must have been even larger than in our experiments, and we therefore consider buckling a plausible candidate to explain the reconstructed oscillations.

In our slab-pull-driven subduction models with a freely moving upper plate we also observe oscillating motion of the trench and upper plate [53]. In our simple experiments, the rigid upper plate is not able to deform, and it thus moves along with the trench where naturally this would lead to changes in stress state, reflected by episodic back-arc spreading [54], extensional or contractional upper plate deformation [35,39,55-60] and even changes in topography [61]. Such variations may be of interest to the understanding of fluid and magmatic processes affecting the upper plate. For instance, episodic magmatic ponding alternating with migration and flare ups [62], and episodic

mineralization [63] and associated pulses in the formation of ore deposits [64] may be the result of such stress state oscillations. Therefore, for subduction zones where slab buckling leads to oscillating trench motion and upper plate deformation, enhanced resolution in marine magnetic anomalies and accompanying reconstructions could lead to a better predictive power in the timing of these magmatic and ore-genesis related upper plate processes. In the Andes, alternations on a timescale of ~10 Ma between shortening and trench retreat were recently postulated to result from slab buckling [60]. For Tibet, the only high-resolution deformation records in the relevant time interval of 60-50 Ma are from the Qiangtang terrane of northern Tibet, far from the trench [65,66], which on a first order appear to record shortening pulses that coincide with the oscillations [19]. More high-resolution work, for instance in the Xigaze forearc basin, could reveal whether the upper plate may also have recorded short periods of extension.

Would all subducting plates then show these oscillating plate motions? Higher-resolution tectonic reconstructions could provide the answer, but we see several reasons why not all ridges that border subducting plates may record such oscillations similarly. The process of buckling at long subduction zones might not occur synchronously along the entire trench. Such a process may explain the oscillating azimuth of India-Asia convergence during the oscillations documented [19]. In addition, subduction rate may vary gradually along-strike of a trench (e.g., the west Pacific subduction zones from New Zealand to Kamchatka), and rapidly across triple junctions (e.g., [67,68]. Plates like the modern Pacific plate would be less susceptible to the effect of slab buckling in the MTZ, even if the oscillations in a 2D system likely occur. We foresee that oscillations in plate motion are best visible for plates where subduction zones are oriented sub-parallel to spreading ridges and sub-perpendicular to the plate motion direction. Possible candidates for the Cenozoic besides the Indian plate are the Nazca plate [60], the Juan de Fuca plate, the Cocos plate, or the Aluk plate [69] and for earlier times perhaps the Farallon or Kula plates. We consider these targets for high-resolution magnetic anomaly reconstruction to further test the possibilities of slab buckling and the opportunities it may apply to understand mantle and lithosphere dynamics and magmatic and economic geology.

Finally, our models show that the rapid oscillations shown by [19] may well be explained by buckling of the subducting slab that results from the accommodation space problem caused by the much lower sinking rates of slabs in the lower mantle. This implies that plate motions that exceed lower mantle slab sinking rates, so larger than 1-1.5 cm/a [22-24], are resisted from the transition zone downwards. In other words, typical plate motions must be primarily driven in the top few hundred kilometers of the mantle. The 410 km phase transition still enhances slab pull, but at the 660 discontinuity the slab encounters resistance and thickens. In addition, the top 100 km of the Earth

also resists plate motion due to friction on the subduction interface or drag resistance from the underlying mantle, therefore plate tectonics must primarily be driven between depths of ~100 and 500 km, or only 6-7% of the Earths radius. This is a remarkably small niche that on Earth apparently has the right conditions for plate tectonics. We foresee that understanding the dynamics of this narrow zone throughout Earth's history holds the key to understand the uniqueness of our planet to start and sustain plate tectonics.

Methods

Model set up

A set of partial differential equations in an extended Boussinesq approximation [70] (EBA) is used to describe our numerical model of subduction. These equations are solved by a finite element method implemented in the SEPRAN package [71,72]. Our model domain is represented by a 2D box 10,000 km wide and 2,000 km deep (Figure 2). The subducting plate stretches from the ridge in the upper left corner to the trench in the middle of the upper surface. The initial temperature distribution in the subducting plate follows a half-space model followed by an adiabatic profile with a potential temperature of 1573 K beneath it.

We carried out two sets of simulations with similar matching parameters. The first set with an overriding plate that is allowed to move freely (subduction with possible rollback), while the second set features a fixed overriding plate (stationary trench – restricted rollback). Figure 3 illustrates time evolution of a reference model for both sets of simulations. In these reference models we assume a subducting and overriding plate age of 100 Ma at the trench and the viscosity of the crustal decoupling layer of $10^{20} Pa \cdot s$.

Models of the first set have a mobile overriding plate with a ridge in the upper right corner. The rollback of trench induces the motion of the entire overriding plate towards the left, which is facilitated by the presence of a hot and low-viscosity mid-ocean ridge. The second set of models has a stagnant overriding plate with an age increasing from approximately ~17 Ma at the right-hand side to 100 Ma (i.e., for the reference model) at the trench. Cold and thus strong overriding plates cannot move to the left because of the impermeable free slip condition on the right vertical boundary. Therefore, rollback is prohibited and the trench remains stagnant during the model run. We evaluated the effects of the age of the subducting and overriding plates [37,56] – we tested ages at the trench ranging from 50 Ma to 200 Ma.

To obtain an initial slab with sufficient negative buoyancy that would facilitate subduction, we first execute a short kinematic run to develop the slab tip to a depth of approximately 200 km. Within this kinematic prerun a constant convergence velocity of 2.5 cm/a is prescribed on the top of

the subducting plate. After 6 Ma the kinematic boundary condition is turned off and an impermeable free slip is prescribed on all boundaries.

Top and bottom model boundaries are considered isothermal with respective temperatures of 273 K and 2132 K while the vertical boundaries have zero heat flux. Thermal diffusivity is constant $10^{-6}\ m^2\ s^{-1}$ while thermal expansivity is depth dependent [73] and decreases from $3 \times 10^{-5}\ K^{-1}$ at the surface to $1.2 \times 10^{-5}\ K^{-1}$ at the bottom of the model domain [74].

We consider the major mantle phase transitions: the polymorphous exothermic transition of forsterite to wadsleyite at 410 km depth and the endothermic transition of ringwoodite to bridgmanite and periclase at a depth of 660 km with their associated petrological density contrasts (Supplementary Table 1). These are incorporated through the harmonic parameterization [75] of a phase function [76]. We performed a parametric study where we varied the values of Clapeyron slopes in a usually accepted range ($\gamma_{410} = 1 - 3$ MPa/K, $\gamma_{660} = -2.5 - (-1.5)$ MPa/K). All these models result in quasiperiodic buckling of the slab. The strengths of the phase transitions control slab dip angle and related rollback velocity, the ability to penetrate the lower mantle as well as slab viscosity in the transition zone. These factors than affect observed periods of the oscillations that vary between ~ 10 – 20 Ma. Based on this parametric study we chose the values of Clapeyron slopes of 3 MPa/k and -1.5 MPa/K for the 410 km and 660 km phase transitions. These values were chosen to accommodate realistic average subduction velocities [25] with fast plate velocity oscillations [19] while still agreeing with in-situ X-ray diffraction experiments and thermodynamic estimates [77-80].

To evaluate the subducting plate velocity and trench retreat velocity in our models we use two passive particles, one initially positioned in the subcrustal lithosphere of the subducting plate (~4600 km left of the trench) and the other one in the overriding plate close to the trench (Figure 2).

Rheological description

Our subduction model incorporates crustal and mantle material. A low-viscosity crustal layer facilitating mechanical decoupling of the subducting and overriding plate is initially positioned along the top of the subducting plate and within the subduction channel (Figure 2). Crustal material is tracked using 2 million tracers prescribed in the crust and its closest vicinity. The initial thickness of the crustal layer is 10 km.

Upper mantle material is described by a composite rheology model [81,82] combining dislocation creep, diffusion creep and a power-law stress limiter which effectively approximates the Peierls creep [83]. In the diffusion and dislocation creep equations (equations 1 and 2), the pressure and temperature dependence of viscosity follows Arrhenius law:

$$\eta_{diff} = A_{diff}{}^{-1}\, exp\left(\frac{E_{diff}+pV_{diff}}{RT}\right) \quad (1)$$

$$\eta_{disl} = A_{disl}{}^{-1/n}\ \dot{\varepsilon}_{||}{}^{(1-n)/n}\, exp\left(\frac{E_{disl}+pV_{disl}}{nRT}\right) \quad (2)$$

$$\eta_y = \sigma_y \dot{\varepsilon_y}{}^{-(1/n_y)} \dot{\varepsilon}_{||}{}^{(1/n_y)-1} \quad (3)$$

$$\frac{1}{\eta_{eff}} = \frac{1}{\eta_{diffl}} + \frac{1}{\eta_{disl}} + \frac{1}{\eta_y}. \quad (4)$$

Here $A_{diff/disl}, E_{diff/disl,}, V_{diff/disl}$ are pre-exponential parameter, activation energy, activation volume for diffusion and dislocation creep, $\dot{\varepsilon}_{||}$ is the second invariant of the strain rate tensor and n is the power-law exponent of the dislocation creep. A power law stress limiter viscosity is parametrized through the yield stress σ_y , reference strain rate $\dot{\varepsilon}_y$ and a power-law exponent n_y , which is set to 10 in our models (equation 3). Assuming unique stress, individual creep mechanism viscosities are combined into the effective viscosity through equation 4.

The lower mantle deformation is assumed to be mainly through diffusion creep [84], therefore we take $\eta_{eff} = \eta_{diff}$ in the lower mantle. Prefactor A_{diff} and activation parameters of lower mantle diffusion creep are based on slab sinking speed analysis [43].

The crust in our models is mostly assumed to have constant viscosity in a range of $\eta_c = 5x10^{19} - 5x10^{20}\ Pa\ s$. We have also conducted several tests with the composite nonlinear rheology of the crust [42] combining dislocation creep [85] and a Byerlee type deformation [86] as an approximation of the brittle failure (pseudoplastic deformation). In these models, dislocation creep viscosity follows equation 5 (similar to equation 2), but the parameters A_c, E_c, V_c and n_c differ from mantle parameters of equation 2 – see table.

$$\eta^c{}_{disl} = A_c{}^{-1/n_c}\ \dot{\varepsilon}_{||}{}^{(1-n_c)/n_c}\, exp\left(\frac{E_c+pV_c}{n_cRT}\right) \quad (5)$$

Pseudoplastic deformation limits the maximum stress in the crust to $\sigma^c{}_y$, where this stress limit increases with lithostatic pressure p through equation 6, here τ_c is the cohesion and μ is the friction coefficient. The pseudoplastic viscosity η_{pl} is then defined by equation 7 and the effective crustal viscosity is given by equation 8.

$$\sigma^c{}_y = \tau_c + \mu p, \quad (6)$$

$$\eta_{pl} = \frac{\sigma^c{}_y}{2\dot{\varepsilon}_{||}}. \quad (7)$$

$$\frac{1}{\eta^c{}_{eff}} = \frac{1}{\eta^c{}_{disl}} + \frac{1}{\eta^c{}_{pl}}. \quad (8)$$

References

1 Forsyth, D. & Uyeda, S. On the relative importance of the driving forces of plate motion. *Geophysical Journal International* **43**, 163-200 (1975).

2 Lithgow-Bertelloni, C. & Richards, M. A. The dynamics of Cenozoic and Mesozoic plate motions. *Reviews of Geophysics* **36**, 27-78 (1998).

3 Behr, W. M. & Becker, T. W. Sediment control on subduction plate speeds. *Earth and Planetary Science Letters* **502**, 166-173 (2018).

4 Coltice, N., Husson, L., Faccenna, C. & Arnould, M. What drives tectonic plates? *Science advances* **5**, eaax4295 (2019).

5 Spakman, W., Chertova, M. V., van den Berg, A. & van Hinsbergen, D. J. Puzzling features of western Mediterranean tectonics explained by slab dragging. *Nature Geoscience* **11**, 211-216 (2018).

6 Müller, R. D. *et al.* A global plate model including lithospheric deformation along major rifts and orogens since the Triassic. *Tectonics* **38**, 1884-1907 (2019).

7 Torsvik, T. H., Müller, R. D., Van der Voo, R., Steinberger, B. & Gaina, C. Global plate motion frames: toward a unified model. *Reviews of geophysics* **46** (2008).

8 Doubrovine, P. V., Steinberger, B. & Torsvik, T. H. Absolute plate motions in a reference frame defined by moving hot spots in the Pacific, Atlantic, and Indian oceans. *Journal of Geophysical Research: Solid Earth* **117** (2012).

9 Müller, R. D. *et al.* A tectonic-rules-based mantle reference frame since 1 billion years ago–implications for supercontinent cycles and plate–mantle system evolution. *Solid Earth* **13**, 1127-1159 (2022).

10 Goes, S., Capitanio, F., Morra, G., Seton, M. & Giardini, D. Signatures of downgoing plate-buoyancy driven subduction in Cenozoic plate motions. *Physics of the Earth and Planetary Interiors* **184**, 1-13 (2011).

11 Sdrolias, M. & Müller, R. D. Controls on back-arc basin formation. *Geochemistry, Geophysics, Geosystems* **7** (2006).

12 Gürer, D., Granot, R. & van Hinsbergen, D. J. Plate tectonic chain reaction revealed by noise in the Cretaceous quiet zone. *Nature Geoscience* **15**, 233-239 (2022).

13 Hu, J., Gurnis, M., Rudi, J., Stadler, G. & Müller, R. D. Dynamics of the abrupt change in Pacific Plate motion around 50 million years ago. *Nature Geoscience* **15**, 74-78 (2022).

14 Bercovici, D., Schubert, G. & Ricard, Y. Abrupt tectonics and rapid slab detachment with grain damage. *Proceedings of the National Academy of Sciences* **112**, 1287-1291 (2015).

15 Knesel, K. M., Cohen, B. E., Vasconcelos, P. M. & Thiede, D. S. Rapid change in drift of the Australian plate records collision with Ontong Java plateau. *Nature* **454**, 754-757 (2008).

16 van Hinsbergen, D. J. *et al.* A record of plume-induced plate rotation triggering subduction initiation. *Nature Geoscience* **14**, 626-630 (2021).

17 van Hinsbergen, D. J., Steinberger, B., Doubrovine, P. V. & Gassmöller, R. Acceleration and deceleration of India-Asia convergence since the Cretaceous: Roles of mantle plumes and continental collision. *Journal of Geophysical Research: Solid Earth* **116** (2011).

18 Wortel, R. & Cloetingh, S. On the origin of the Cocos-Nazca spreading center. *Geology* **9**, 425-430 (1981).
19 DeMets, C. & Merkouriev, S. Detailed reconstructions of India–Somalia Plate motion, 60 Ma to present: implications for Somalia Plate absolute motion and India–Eurasia Plate motion. *Geophysical Journal International* **227**, 1730-1767 (2021).
20 Patriat, P. & Achache, J. India–Eurasia collision chronology has implications for crustal shortening and driving mechanism of plates. *Nature* **311**, 615-621 (1984).
21 White, L. T. & Lister, G. S. The collision of India with Asia. *Journal of Geodynamics* **56**, 7-17 (2012).
22 Van Der Meer, D. G., Spakman, W., Van Hinsbergen, D. J., Amaru, M. L. & Torsvik, T. H. Towards absolute plate motions constrained by lower-mantle slab remnants. *Nature Geoscience* **3**, 36-40, doi:10.1038/ngeo708 (2010).
23 Van der Meer, D. G., Van Hinsbergen, D. J. & Spakman, W. Atlas of the underworld: Slab remnants in the mantle, their sinking history, and a new outlook on lower mantle viscosity. *Tectonophysics* **723**, 309-448, doi:10.1016/j.tecto.2017.10.004 (2018).
24 Butterworth, N. *et al.* Geological, tomographic, kinematic and geodynamic constraints on the dynamics of sinking slabs. *Journal of Geodynamics* **73**, 1-13, doi:10.1016/j.jog.2013.10.006 (2014).
25 Zahirovic, S., Müller, R. D., Seton, M. & Flament, N. Tectonic speed limits from plate kinematic reconstructions. *Earth and Planetary Science Letters* **418**, 40-52, doi:10.1016/j.epsl.2015.02.037 (2015).
26 Goes, S., Agrusta, R., van Hunen, J. & Garel, F. Subduction-transition zone interaction: A review. *Geosphere* **13**, 644-664 (2017).
27 Sigloch, K. & Mihalynuk, M. G. Intra-oceanic subduction shaped the assembly of Cordilleran North America. *Nature* **496**, 50-56 (2013).
28 Ribe, N. M., Stutzmann, E., Ren, Y. & Van Der Hilst, R. Buckling instabilities of subducted lithosphere beneath the transition zone. *Earth and Planetary Science Letters* **254**, 173-179 (2007).
29 Wu, J., Suppe, J., Lu, R. & Kanda, R. Philippine Sea and East Asian plate tectonics since 52 Ma constrained by new subducted slab reconstruction methods. *Journal of Geophysical Research: Solid Earth* **121**, 4670-4741 (2016).
30 Chen, Y.-W., Wu, J. & Suppe, J. Southward propagation of Nazca subduction along the Andes. *Nature* **565**, 441-447 (2019).
31 Van der Voo, R., Spakman, W. & Bijwaard, H. Tethyan subducted slabs under India. *Earth and Planetary Science Letters* **171**, 7-20, doi:10.1016/S0012-821X(99)00131-4 (1999).
32 Replumaz, A., Karason, H., van der Hilst, R. D., Besse, J. & Tapponnier, P. 4-D evolution of SE Asia's mantle from geological reconstructions and seismic tomography. *Earth and Planetary Science Letters* **221**, 103-115 (2004).
33 Parsons, A. J., Sigloch, K. & Hosseini, K. Australian Plate Subduction is Responsible for Northward Motion of the India-Asia Collision Zone and∼ 1,000 km Lateral Migration of the Indian Slab. *Geophysical Research Letters* **48**, e2021GL094904, doi:10.1029/2021GL094904 (2021).
34 Qayyum, A. *et al.* Subduction and Slab Detachment Under Moving Trenches During Ongoing India-Asia Convergence. *Geochemistry, Geophysics, Geosystems* **23**, e2022GC010336 (2022).

35 Billen, M. I. & Arredondo, K. M. Decoupling of plate-asthenosphere motion caused by non-linear viscosity during slab folding in the transition zone. *Physics of the Earth and Planetary Interiors* **281**, 17-30 (2018).
36 Čížková, H. & Bina, C. R. Effects of mantle and subduction-interface rheologies on slab stagnation and trench rollback. *Earth and Planetary Science Letters* **379**, 95-103 (2013).
37 Garel, F. *et al.* Interaction of subducted slabs with the mantle transition-zone: A regime diagram from 2-D thermo-mechanical models with a mobile trench and an overriding plate. *Geochemistry, Geophysics, Geosystems* **15**, 1739-1765 (2014).
38 Holt, A. F., Becker, T. & Buffett, B. Trench migration and overriding plate stress in dynamic subduction models. *Geophysical Journal International* **201**, 172-192 (2015).
39 Lee, C. & King, S. D. Dynamic buckling of subducting slabs reconciles geological and geophysical observations. *Earth and Planetary Science Letters* **312**, 360-370 (2011).
40 Schellart, W. P. Influence of the subducting plate velocity on the geometry of the slab and migration of the subduction hinge. *Earth and Planetary Science Letters* **231**, 197-219 (2005).
41 Xue, K., Schellart, W. P. & Strak, V. Overriding plate deformation and topography during slab rollback and slab rollover: insights from subduction experiments. *Tectonics* **41**, e2021TC007089 (2022).
42 Pokorný, J., Čížková, H. & van den Berg, A. Feedbacks between subduction dynamics and slab deformation: Combined effects of nonlinear rheology of a weak decoupling layer and phase transitions. *Physics of the Earth and Planetary Interiors* **313**, 106679 (2021).
43 Čížková, H., van den Berg, A. P., Spakman, W. & Matyska, C. The viscosity of Earth's lower mantle inferred from sinking speed of subducted lithosphere. *Physics of the earth and Planetary Interiors* **200**, 56-62, doi:10.1016/j.pepi.2012.02.010 (2012).
44 Čížková, H. & Bina, C. R. Linked influences on slab stagnation: Interplay between lower mantle viscosity structure, phase transitions, and plate coupling. *Earth and Planetary Science Letters* **509**, 88-99 (2019).
45 Běhounková, M. & Čížková, H. Long-wavelength character of subducted slabs in the lower mantle. *Earth and Planetary Science Letters* **275**, 43-53 (2008).
46 Capitanio, F., Faccenna, C., Zlotnik, S. & Stegman, D. Subduction dynamics and the origin of Andean orogeny and the Bolivian orocline. *Nature* **480**, 83-86 (2011).
47 Behr, W. M., Holt, A. F., Becker, T. W. & Faccenna, C. The effects of plate interface rheology on subduction kinematics and dynamics. *Geophysical Journal International* **230**, 796-812 (2022).
48 Van Der Meer, D. G. *et al.* Plate tectonic controls on atmospheric CO2 levels since the Triassic. *Proceedings of the National Academy of Sciences* **111**, 4380-4385, doi:10.1073/pnas.1315657111 (2014).
49 Espinoza, V. & Iaffaldano, G. Rapid absolute plate motion changes inferred from high-resolution relative spreading reconstructions: A case study focusing on the South America plate and its Atlantic/Pacific neighbors. *Earth and Planetary Science Letters* **604**, 118009 (2023).
50 Kumar, P. *et al.* The rapid drift of the Indian tectonic plate. *Nature* **449**, 894-897 (2007).
51 van Hinsbergen, D. J. *et al.* Reconstructing Greater India: Paleogeographic, kinematic, and geodynamic perspectives. *Tectonophysics* **760**, 69-94 (2019).

52 Stegman, D. R., Farrington, R., Capitanio, F. A. & Schellart, W. P. A regime diagram for subduction styles from 3-D numerical models of free subduction. *Tectonophysics* **483**, 29-45 (2010).
53 Royden, L. H. & Husson, L. Trench motion, slab geometry and viscous stresses in subduction systems. *Geophysical Journal International* **167**, 881-905, doi:10.1111/j.1365-246X.2006.03079.x (2006).
54 Ishii, K. & Wallis, S. R. A possible mechanism for spontaneous cyclic back-arc spreading. *Progress in Earth and Planetary Science* **9**, 27 (2022).
55 Boutoux, A. *et al.* Slab folding and surface deformation of the Iran mobile belt. *Tectonics* **40**, e2020TC006300 (2021).
56 Capitanio, F. A., Stegman, D. R., Moresi, L.-N. & Sharples, W. Upper plate controls on deep subduction, trench migrations and deformations at convergent margins. *Tectonophysics* **483**, 80-92 (2010).
57 Cerpa, N. G., Guillaume, B. & Martinod, J. The interplay between overriding plate kinematics, slab dip and tectonics. *Geophysical Journal International* **215**, 1789-1802 (2018).
58 Dasgupta, R., Mandal, N. & Lee, C. Controls of subducting slab dip and age on the extensional versus compressional deformation in the overriding plate. *Tectonophysics* **801**, 228716 (2021).
59 Van Hinsbergen, D. J. & Schouten, T. L. Deciphering paleogeography from orogenic architecture: constructing orogens in a future supercontinent as thought experiment. *American Journal of Science* **321**, 955-1031 (2021).
60 Pons, M., Sobolev, S. V., Liu, S. & Neuharth, D. Hindered trench migration due to slab steepening controls the formation of the Central Andes. *Journal of Geophysical Research: Solid Earth*, e2022JB025229 (2022).
61 Briaud, A., Agrusta, R., Faccenna, C., Funiciello, F. & van Hunen, J. Topographic fingerprint of deep mantle subduction. *Journal of Geophysical Research: Solid Earth* **125**, e2019JB017962 (2020).
62 Chapman, J. B. *et al.* The causes of continental arc flare ups and drivers of episodic magmatic activity in Cordilleran orogenic systems. *Lithos* **398**, 106307 (2021).
63 Chelle-Michou, C., Chiaradia, M., Selby, D., Ovtcharova, M. & Spikings, R. A. High-resolution geochronology of the Coroccohuayco porphyry-skarn deposit, Peru: A rapid product of the Incaic orogeny. *Economic Geology* **110**, 423-443 (2015).
64 Wilson, C. J., Moore, D. H., Vollgger, S. A. & Madeley, H. E. Structural evolution of the orogenic gold deposits in central Victoria, Australia: The role of regional stress change and the tectonic regime. *Ore Geology Reviews* **120**, 103390 (2020).
65 Li, S. *et al.* Does pulsed Tibetan deformation correlate with Indian plate motion changes? *Earth and Planetary Science Letters* **536**, 116144 (2020).
66 Li, S. *et al.* Anisotropy of magnetic susceptibility (AMS) analysis of the Gonjo Basin as an independent constraint to date Tibetan shortening pulses. *Geophysical Research Letters* **47**, e2020GL087531 (2020).
67 van de Lagemaat, S. H., Van Hinsbergen, D. J., Boschman, L. M., Kamp, P. J. & Spakman, W. Southwest Pacific absolute plate kinematic reconstruction reveals major Cenozoic Tonga-Kermadec slab dragging. *Tectonics* **37**, 2647-2674 (2018).
68 Vaes, B., Van Hinsbergen, D. J. & Boschman, L. M. Reconstruction of subduction and back-arc spreading in the NW Pacific and Aleutian Basin: Clues to causes of Cretaceous and Eocene plate reorganizations. *Tectonics* **38**, 1367-1413 (2019).

69 van de Lagemaat, S. H., Kamp, P. J., Boschman, L. M. & Van Hinsbergen, D. J. Reconciling the Cretaceous breakup and demise of the Phoenix Plate with East Gondwana orogenesis in New Zealand. *Earth-Science Reviews*, 104276 (2023).
70 Ita, J. & King, S. D. Sensitivity of convection with an endothermic phase change to the form of governing equations, initial conditions, boundary conditions, and equation of state. *Journal of Geophysical Research: Solid Earth* **99**, 15919-15938 (1994).
71 van den Berg, A., Segal, G. & Yuen, D. A. SEPRAN: A versatile finite-element package for a wide variety of problems in geosciences. *Journal of Earth Science* **26**, 89-95 (2015).
72 Segal, A. & Praagman, N. The sepran fem package. *Tech. Report, Ingenieursbureau Sepra, Netherlands* (2005).
73 Katsura, T. *et al.* Thermal expansion of forsterite at high pressures determined by in situ X-ray diffraction: The adiabatic geotherm in the upper mantle. *Physics of the Earth and Planetary Interiors* **174**, 86-92 (2009).
74 Hansen, U., Yuen, D., Kroening, S. & Larsen, T. Dynamical consequences of depth-dependent thermal expansivity and viscosity on mantle circulations and thermal structure. *Physics of the earth and planetary interiors* **77**, 205-223 (1993).
75 Čížková, H., van Hunen, J. & van den Berg, A. Stress distribution within subducting slabs and their deformation in the transition zone. *Physics of the Earth and Planetary Interiors* **161**, 202-214 (2007).
76 Christensen, U. R. & Yuen, D. A. Layered convection induced by phase transitions. *Journal of Geophysical Research: Solid Earth* **90**, 10291-10300 (1985).
77 Morishima, H. *et al.* The phase boundary between α-and β-Mg2SiO4 determined by in situ X-ray observation. *Science* **265**, 1202-1203 (1994).
78 Bina, C. R. & Helffrich, G. Phase transition Clapeyron slopes and transition zone seismic discontinuity topography. *Journal of Geophysical Research: Solid Earth* **99**, 15853-15860 (1994).
79 Katsura, T. *et al.* Olivine-wadsleyite transition in the system (Mg, Fe) 2SiO4. *Journal of Geophysical Research: Solid Earth* **109** (2004).
80 Su, C. *et al.* Thermodynamic Properties of Fe-Bearing Wadsleyite and Determination of the Olivine-Wadsleyite Phase Transition Boundary in (Mg, Fe) 2SiO4 System. *Frontiers in Earth Science* **10**, 879678 (2022).
81 Čížková, H., van Hunen, J., van den Berg, A. P. & Vlaar, N. J. The influence of rheological weakening and yield stress on the interaction of slabs with the 670 km discontinuity. *Earth and Planetary Science Letters* **199**, 447-457 (2002).
82 van den Berg, A. P., van Keken, P. E. & Yuen, D. A. The effects of a composite non-Newtonian and Newtonian rheology on mantle convection. *Geophysical Journal International* **115**, 62-78 (1993).
83 Androvičová, A., Čížková, H. & van den Berg, A. The effects of rheological decoupling on slab deformation in the Earth's upper mantle. *Studia Geophysica et Geodaetica* **57**, 460-481 (2013).
84 Karato, S.-i., Zhang, S. & Wenk, H.-R. Superplasticity in Earth's lower mantle: evidence from seismic anisotropy and rock physics. *Science* **270**, 458-461 (1995).
85 Ranalli, G. *Rheology of the Earth*. (Springer Science & Business Media, 1995).
86 Karato, S.-i. Deformation of earth materials. *An introduction to the rheology of Solid Earth* **463** (2008).

Acknowledgements

Netherlands Organisation for Scientific Research, NWO Vici Grant 865.17.001 (EvdW, DJJvH)

Charles University Grant Agency, grant number 36121 (JP), grant SVV 260709 (JP, HC)

Czech Science Foundation, grant 23-06345S (JP, HC). We thank Craig R. Bina for fruitful discussions.

Open Research

All modelling data that is used to produces the figures in this manuscript can be found on Zenodo:

10.5281/zenodo.10159525

Author contributions

Conceptualization: EvdW, JP, DJJvH

Methodology: EvdW, JP, HC, APvdB

Investigation: EvdW, JP

Visualization: EvdW, JP

Supervision: HC, DJJvH

Writing – original draft: EvdW, JP

Writing – review & editing: all authors

Competing interests:

Authors declare that they have no competing interests.

Figure legends

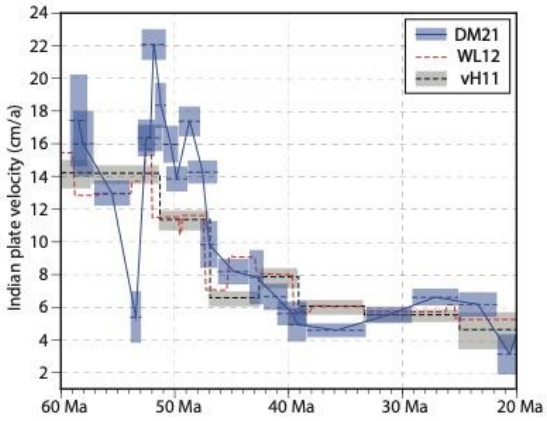

Figure 1 – Indian plate motion history

Indian plate velocity relative to Eurasia from 60 Ma ago to 20 Ma ago. Shown are the reconstructed velocities of the Indian plate from DM21 [19], WL12 [21] and vH11 [17]. Blue and grey rectangles indicate error margins in reconstructions and time interval spanned by each stage velocity.

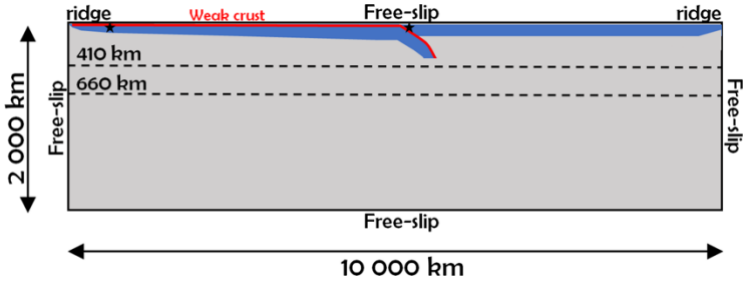

Figure 2 – Model setup

Model domain is 10 000 km wide and 2000 km deep. Dashed lines indicate major phase transitions at 410 and 660 km depth. Red line positioned at the top of the subducting slab indicates a 10 km thick weak crustal layer, effectively separating the plates. Two black asterisks represent tracers used to track the velocity of the subducting plate and overriding plate. Free slip boundary condition is prescribed on all boundaries.

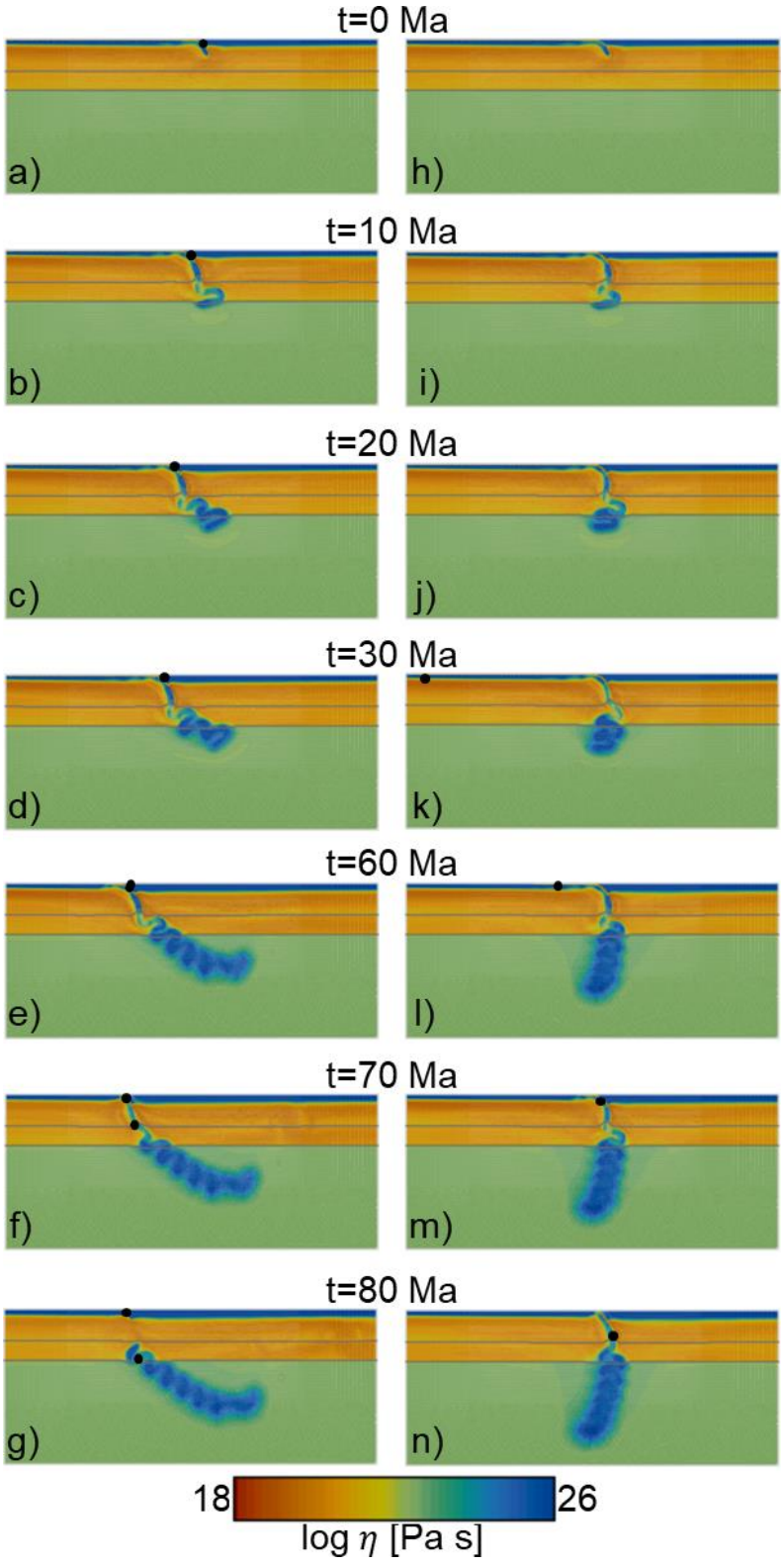

Figure 3 – Time evolution of the reference models

Zoomed-in viscosity snapshots (4800x2000 km) of the model for 80 Ma of model time. Grey lines indicate position of the major phase transition at 410 and 660 km depth with the values of Clapeyron slopes of 3 and -1.5 MPa/K, respectively. Black dots are reference points used to calculate plate velocities. a-g) Reference model with free moving overriding plate resulting in trench retreat and an inclined slab in the lower mantle. h-n) Reference model with a stationary trench creating a vertical lower mantle slab.

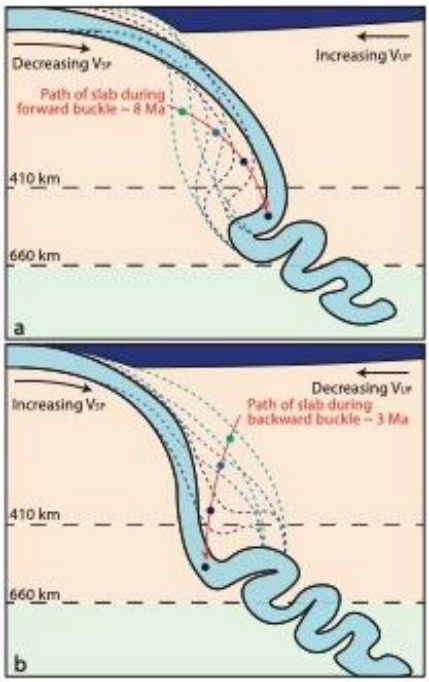

Figure 4 – Illustrated effect of slab buckling on upper mantle slab geometry

A cartoon illustrating forward (a) and backward (b) slab buckling as result of the interplay of the slab with the phase transitions and the lower mantle. During forward buckling the slab in the MTZ advances while the trench retreats, accompanied by a decreasing V_{SP} and increasing V_{UP}. The backward buckle allows the slab to sink fast in the MTZ with a rapid increase of V_{SP}, while the trench stays mantle stationary. The backward buckles form faster than forward buckles, in about 3 versus 8 Ma for our reference model.

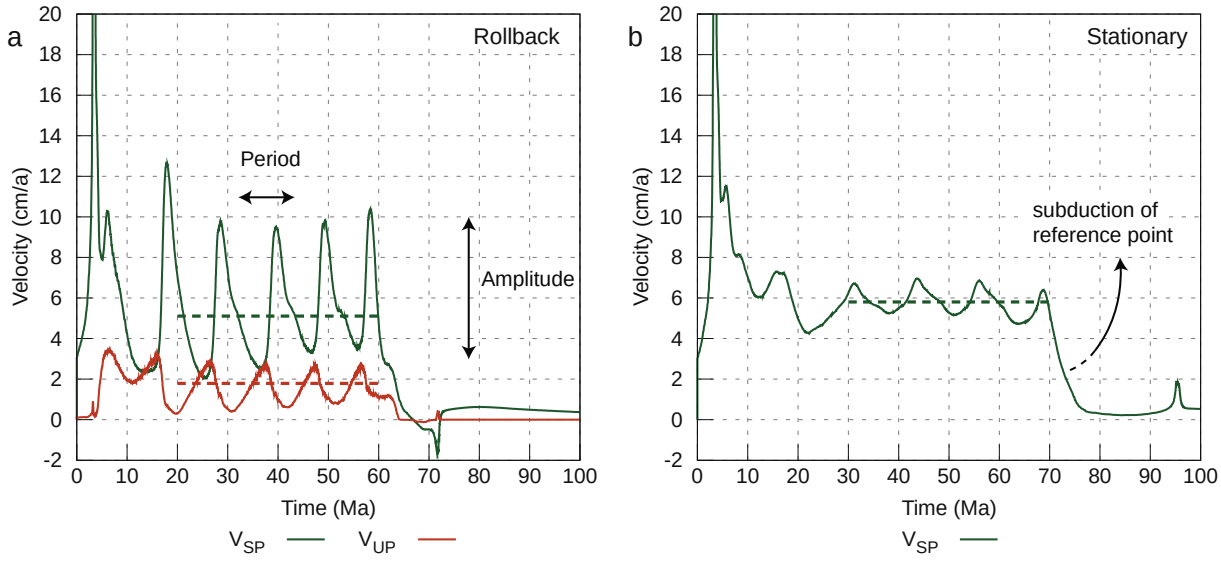

Figure 5 – Plate motion oscillations

Temporal evolution of the plate motions in both reference models. a) Subduction velocity and overriding plate motion of the reference model with rollback, V_{SP} oscillates between 2 and 10 cm/a and V_{UP} between 0 and 3 cm/a. The reference point subducts at t = 60 Ma and slab detachment occurs around t = 70 Ma. b) Similar as in a but for the reference model with a stationary trench, subduction of the reference point occurs at t = 70 Ma and slab detachment at t = 90 Ma. The dashed lines indicate the average velocity, which is calculated over the shown 40 Ma time-interval.

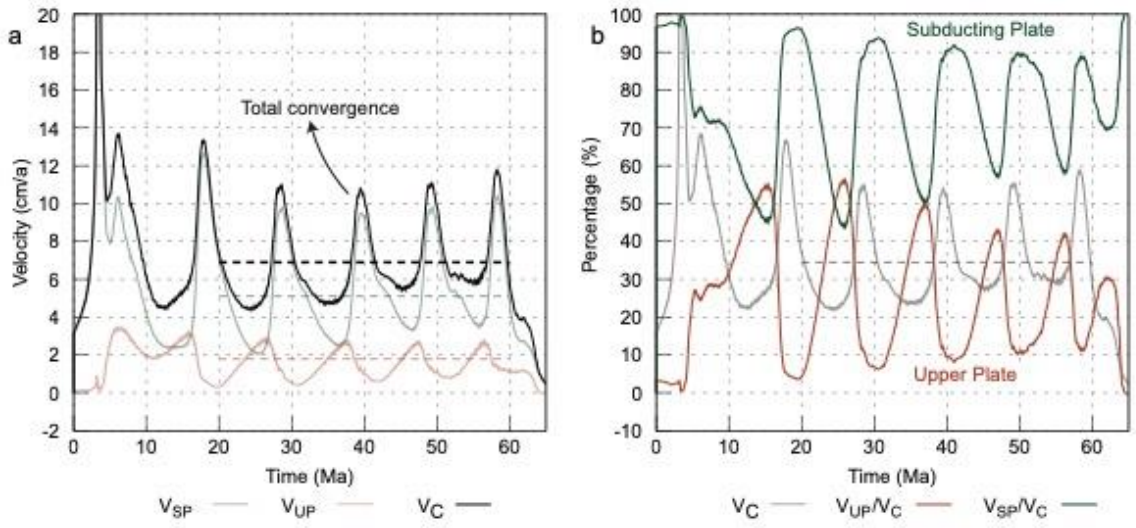

Figure 6 – Total convergence rate

a) Total convergence rate ($V_C = V_{SP} + V_{UP}$) of the reference model with rollback showing smaller amplitudes in the oscillations, red and green lines are the same as in Figure 5a. b) Relative percentages of the total convergence rate for both the subducting plate (green; 100-50%) and overriding plate (orange; 50-0%). Grey line is the same as in a, and uses the y-axis of a.

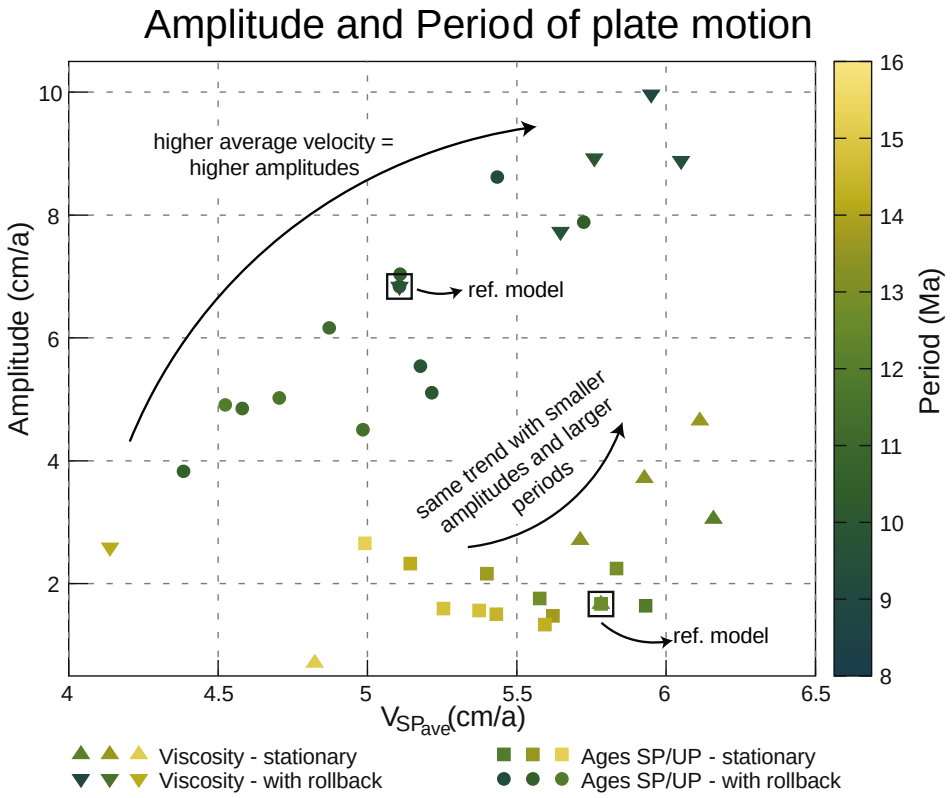

Figure 7 – Amplitude and Period of the subducting plate motion

Overview of all models showing the relation the amplitude and period (colour) of V_{SP} oscillations have with the average V_{SP}. The four types of models shown are with a varying crustal viscosity and rollback (triangles) or a stationary trench (upside-down triangles), and models with changing SP and UP ages with rollback (circles) or a stationary trench (squares). For values of the crustal viscosity and ages of plates see figure 8.

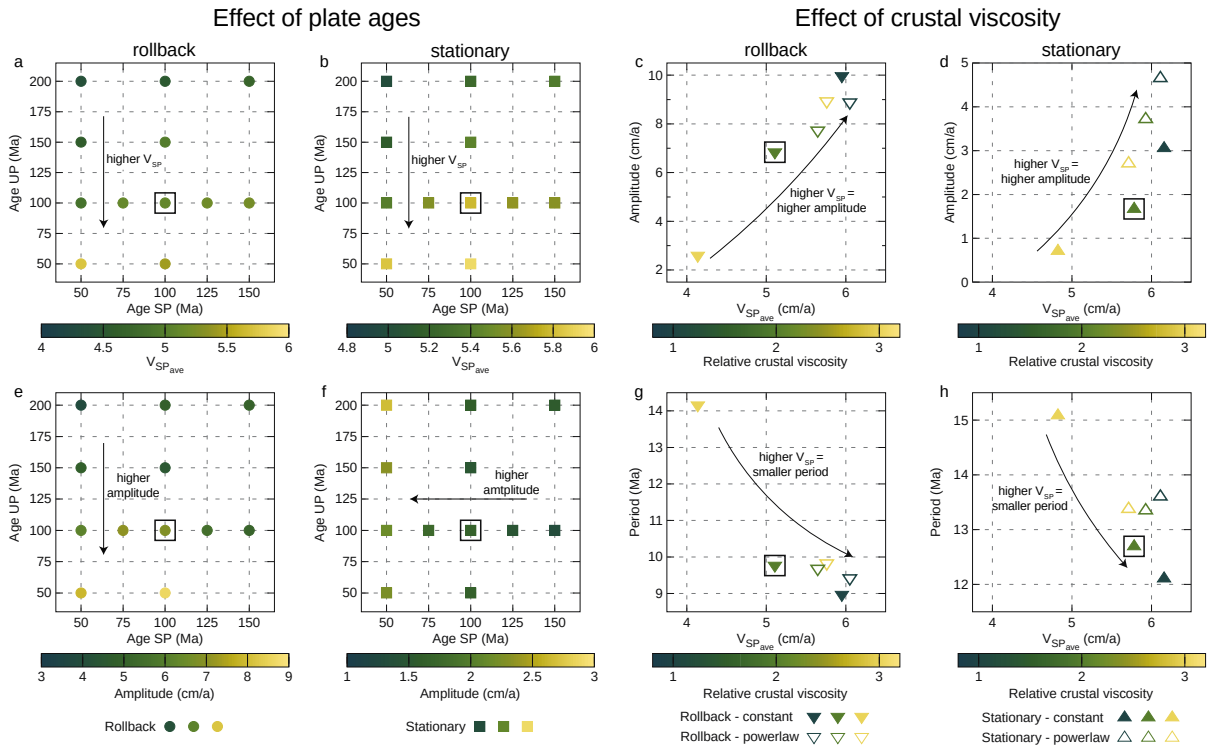

Figure 8 – Amplitude, Period and V_{SP} as function of plate age and crustal viscosity

V_{SP} as function of SP and OP ages for models with a moving trench (a) and a stationary trench (b). Amplitude of the oscillating V_{SP} as function of the average V_{SP} for crustal viscosities: 5e19, 1e20, 5e20 (closed triangles) and three power law crustal viscosities (open triangles) in models with a moving trench (c) and a stationary trench (d). Amplitude of the oscillating V_{SP} as function of SP and OP plate ages for models with a moving trench (e) and a stationary trench (f). Period of the oscillating V_{SP} as function of the average V_{SP} for a varying crustal viscosity in models with a moving trench (g) and a stationary trench (h).

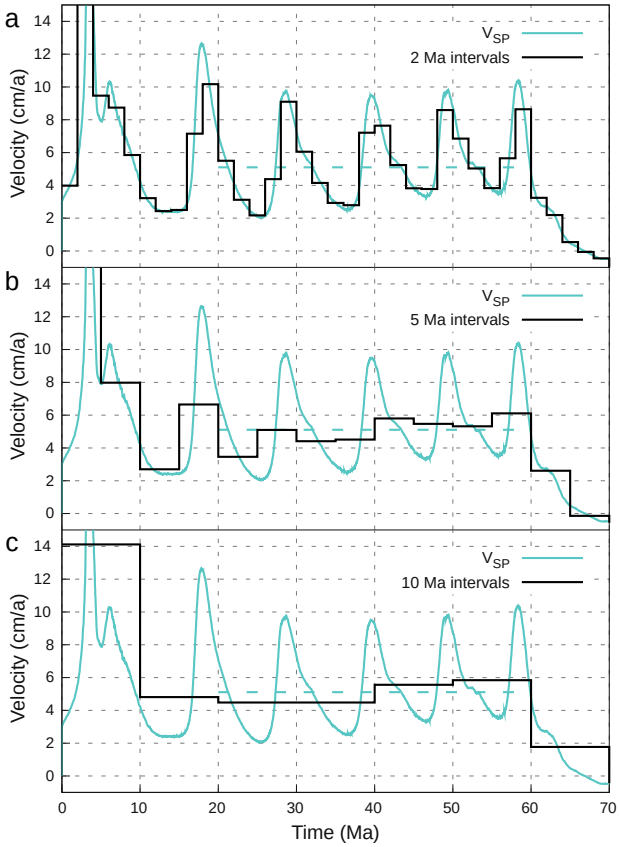

Figure 9 – Sampling intervals for subducting plate velocity

Horizontal subducting plate motion for the reference model with rollback and stage velocities if sampled at 2, 5 or 10 Ma intervals.

Supplementary Table

Table 1 – Model parameters

Table 1
Model parameters

symbol	Meaning	Value	Units
Upper mantle and oceanic lithosphere rheology			
A_{diff}	Pre-exponential parameter of diffusion creep[a]	1×10^{-9}	$Pa^{-1}\ s^{-1}$
A_{disl}	Pre-exponential parameter of dislocation creep[a]	31.5×10^{-18}	$Pa^{-n}\ s^{-1}$
E_{diff}	Activation energy of diffusion creep[a]	3.35×10^{5}	$J\ mol^{-1}$
E_{disl}	Activation energy of dislocation creep[a]	4.8×10^{5}	$J\ mol^{-1}$
V_{diff}	Activation volume of diffusion creep[a]	4.0×10^{-6}	$m^3\ mol^{-1}$
V_{disl}	Activation volume of dislocation creep[a]	11×10^{-6}	$m^3\ mol^{-1}$
η_{diff}	Viscosity of diffusion creep	–	$Pa\ s$
η_{disl}	Viscosity of dislocation creep	–	$Pa\ s$
η_y	Power-law stress limitor viscosity	–	$Pa\ s$
n	dislocation creep exponent	3.5	–
$\dot{\epsilon}_y$	Reference strain rate	1×10^{-15}	s^{-1}
σ_y	Stress limit	$2 - 5 \times 10^{8}$	Pa
p	Hydrostatic pressure	–	Pa
n_y	Stress limit exponent	10	–
R	Gas constant	8.314	$J\ K^{-1}\ mol^{-1}$
T	Temperature	–	K
$\dot{\epsilon}_{\|\|}$	Second invariant of strainrate	–	s^{-1}
Lower mantle rheology			
A_{diff}	Pre-exponential parameter of diffusion creep	1.3×10^{-16}	$Pa^{-1}\ s^{-1}$
E_{diff}	Activation energy of diffusion creep[b]	2×10^{5}	$J\ mol^{-1}$
V_{diff}	Activation volume of diffusion creep[b]	1.1×10^{-6}	$m^3\ mol^{-1}$
Other model parameters			
η_c	Range of constant viscosity crust values	$5 \times 10^{19} - 5 \times 10^{20}$	$Pa\ s$
κ	Thermal diffusivity	10^{-6}	$m^2\ s^{-1}$
g	Gravitational acceleration	9.8	$m^2\ s^{-2}$
ρ_0	Reference density	3416	$kg\ m^{-3}$
c_p	Specific heat	1250	$J\ kg^{-1}\ K^{-1}$
α_0	Surface thermal expansivity	3×10^{-5}	K^{-1}
γ_{410}	Clapeyron slope of 410 km phase transition[c]	3×10^{6}	$Pa\ K^{-1}$
γ_{660}	Clapeyron slope of 660 km phase transition[c]	-1.5×10^{6}	$Pa\ K^{-1}$
$\delta_{\rho 410}$	Density contrast of 410 km phase transition[d]	273	$kg\ m^{-3}$
$\delta_{\rho 660}$	Density contrast of 660 km phase transition[d]	341	$kg\ m^{-3}$
Nonlinear crustal rheology			
A_c	Pre-exponential parameter of dislocation creep	2.5×10^{-17}	$Pa^{-1}\ s^{-1}$
E_c	Activation energy of dislocation creep	1.54×10^{5}	$J\ mol^{-1}$
V_c	Activation volume of dislocation creep	0	$m^3\ mol^{-1}$
n_c	dislocation creep exponent	2.3	–
τ_c	Cohesion	$0.25 - 1 \times 10^{7}$	Pa
μ_c	Friction coefficient	$0.025 - 0.1$	–
σ_y^c	Stress limit in the crust	–	Pa

(a) Parameters of wet olivine based on Hirth and Kohstedt (2003).
(b) Čížková et al. (2012).
(c) Bina and Helffrich (1994).
(d) Steinbach and Yuen (1995).